

Microwave emission by a spin Hall nano-oscillator

R. H. Liu, W. L. Lim, and S. Urazhdin

Department of Physics, Emory University, Atlanta, GA 30322

We study the effects of a pure spin current on the magnetization of a Permalloy film. The spin current is generated due to the spin Hall effect by locally injecting an in-plane electric current into an adjacent Pt layer. Microwave spectroscopy shows that the spin current induces coherent oscillations of the magnetization of Permalloy, resulting in emission of microwave radiation due to the anisotropic magnetoresistance. The frequency of the emitted microwaves is always lower than the ferromagnetic resonance frequency of the ferromagnet, indicating that the oscillation forms a non-propagating spin wave "bullet". Our measurements demonstrate the viability of active magnetoelectronic microwave devices operated by pure spin currents.

PACS numbers: 76.50.+g, 75.75.-c, 75.30.Ds

Spin-polarized electric currents can be utilized to modify the magnetic configuration of ferromagnets and are thus essential for the operation of active spin-based electronic (spintronic) devices [1]. These devices typically utilize two ferromagnetic layers [2]. The electric current is spin-polarized in one layer and injected into another (free) layer, changing the magnetic configuration or causing microwave-frequency precession of the latter due to the spin torque (ST) effect [3–6]. The ST exerted by each transmitted electron is generally limited by its total spin-angular momentum $\hbar/2$. As a consequence, device operation requires a relatively large electric current I that scales with the magnetic moment of the free ferromagnet [3]. On the other hand, the thermal stability of nanoscale magnetic devices generally improves with increasing magnetic moment [7]. Because of these opposite trends, achieving a balance between efficiency and stability of spin torque devices is challenging.

In a recently developed class of spintronic devices, the spin Hall effect (SHE) [8, 9] produces a pure spin current controlling the magnetization of ferromagnets [10–14]. The efficiency of SHE devices is not limited by the magnitude of the angular momentum of electron, since a single electron passing through the device can experience multiple scattering both in the ferromagnet and in the SHE material, transferring a sizable fraction of its total angular momentum in each scattering event. Moreover, since electric current does not need to flow through the active magnetic layer, SHE devices can utilize not only conducting but also dielectric magnetic materials.

While the use of SHE opens possibilities for new device geometries, it also requires innovative approaches to signal generation taking advantage of magnetoresistance effects that do not necessarily require an additional magnetic layer. Development of active SHE devices also requires a better understanding of the effects of geometry on the dynamical characteristics of magnetic systems. For instance, it has been demonstrated that magnetization oscillations cannot be induced by a uniform spin current applied to a micron-sized ferromagnetic disk because of the nonlinear damping [12].

Auto-oscillation induced by SHE has been recently observed by micro-focus Brillouin light spectroscopy (BLS) in an in-plane point-contact geometry. By locally injecting a spin current into an extended magnetic film [15], radiative damping of the propagating spin-wave modes was enhanced, suppressing nonlinear processes and enabling auto-oscillation. These measurements demonstrated a route for achieving oscillations due to SHE, but did not show how these oscillations can be converted into microwave signals. The spectroscopic resolution of BLS was also insufficient to determine the spectral properties of the oscillation.

Here, we demonstrate coherent microwave generation due to the SHE in a device that utilizes local current injection to suppress nonlinear damping, and anisotropic magnetoresistance (AMR) of the magnetic layer to convert the oscillations into a microwave signal. Our spectroscopic measurements directly demonstrate the coherent single-mode nature of the excitation and confirm its relation to the spin-wave spectrum observed in Ref. [15]. Finally, we show that all the oscillation characteristics exhibit a strong dependence on temperature, suggesting that thermal fluctuations significantly affect both the SHE and the oscillation itself.

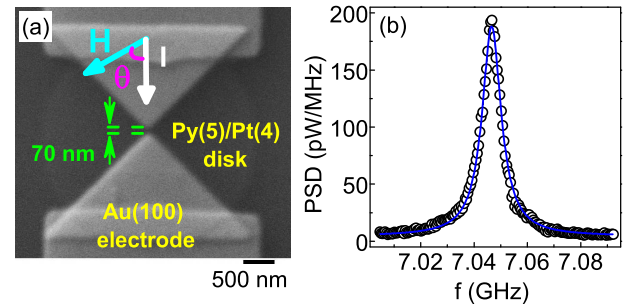


FIG. 1: (Color online). (a) Scanning electron micrograph of the test device. (b) Symbols: power spectral density (PSD) of the microwave signal emitted by the device at $H = 700$ Oe, $I = 20$ mA, $T = 6$ K, at an angle $\theta = 60^\circ$ between the direction of the field and the current flow. The curve is the result of fitting by the Lorentzian function.

Figure 1(a) shows a scanning electron microscopy (SEM) image of our test device and the experimental layout. The device is comprised of a $4\text{ }\mu\text{m}$ Py(5)/Pt(4) bilayer disk and two pointed Au(100) electrodes on top. Here, Py is Permalloy ($\text{Ni}_{80}\text{Fe}_{20}$), and thicknesses are in nanometers. The device was fabricated by a combination of sputtering and e-beam lithography. The separation between the endpoints of the Au electrodes was 70 nm . By applying a voltage between the Au electrodes, an in-plane electrical current localized mostly in the gap between electrodes was induced in the Py/Pt bilayer. This current induced a pure spin current flowing towards the Py layer due to the SHE in Pt [8, 9], resulting in the oscillation of the Py magnetization \mathbf{M} .

To enable microwave generation due to this oscillation, we utilized the dependence of the device resistance R on the angle θ between \mathbf{M} and the direction of current I . The sinusoidal dependence of R on θ with a period of 180° was consistent with the anisotropic magnetoresistance (AMR) of Py [16]. The relative magnetoresistance was $\Delta R/R = [R(0^\circ) - R(90^\circ)]/R(90^\circ) = 0.125\%$ at RT, which was an order of magnitude smaller than in standalone Py films due to shunting by Pt.

Previous studies showed that the current-induced excitation is most efficient when the magnetic field H , the direction of the current flow, and the normal to the film surface directed from Py to Pt form a right-hand set of orthogonal vectors [12, 14], consistent with the expected symmetry of SHE [8, 9]. On the other hand, the AMR has a minimum when \mathbf{H} is orthogonal to I , and therefore a microwave signal at the oscillation frequency cannot be produced in this configuration. This limitation of AMR can be avoided by choosing intermediate orientations of \mathbf{H} such that the oscillation of \mathbf{M} can be induced by the spin torque, and simultaneously a microwave signal can be generated at the frequency of the oscillation. We observed oscillations in the range of θ between 30° and 85° , as illustrated in Fig. 1(b) for $\theta = 60^\circ$. The spectrum can be well fitted by the Lorentzian function with a full width at half maximum (FWHM) of 5 MHz at $T = 6\text{ K}$ [solid curve in Fig. 1(b)]. The actual temperature of the active device area was $T_a \approx 50\text{ K}$ because of the Joule heating, as discussed below.

Figure 2 shows the dependence of the generation characteristics on current I at $T = 120\text{ K}$. A small oscillation peak appeared at $I > 14\text{ mA}$. The intensity of the peak quickly increased to a maximum amplitude of 110 pW/MHz at $I = 19\text{ mA}$ and the frequency slightly increased, while the linewidth decreased to a minimum value of 10 MHz at $I = 19\text{ mA}$. At $I > 19\text{ mA}$, the peak broadened and decreased in amplitude while shifting to lower frequencies. This evolution of the oscillation characteristics is remarkably similar to the traditional spin-valve nano-oscillators both in the nanopillar [17] and point contact geometries [18, 19]. It is consistent with the theory of nonlinear oscillators, which predicts that the

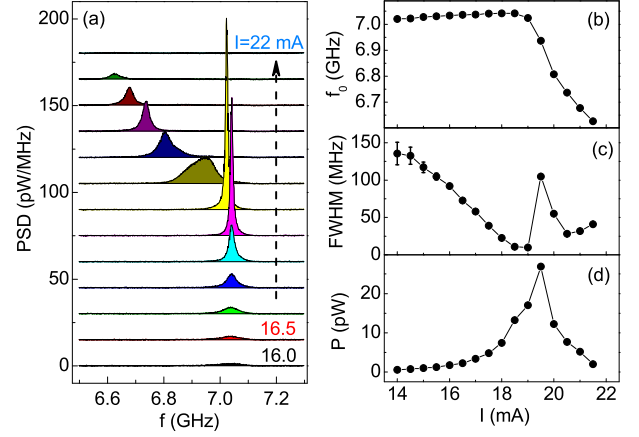


FIG. 2: (Color online). Dependence of the microwave generation characteristics on current, at $H = 700\text{ Oe}$, $\theta = 60^\circ$, $T = 120\text{ K}$. (a) Generation spectra at I between 16 mA and 22 mA varied in 0.5 mA steps. (b)-(d) Dependence of the central generation frequency (b), FWHM (c) and integral intensity (d) on current. The central frequency and the linewidth were determined by fitting the power spectra with the Lorentzian function.

thermal linewidth decreases with increasing oscillation power and increases with increasing nonlinearity [20, 21]. In particular, the minimum of the linewidth corresponding to the peak of the oscillation frequency at $I = 19\text{ mA}$ can be attributed to the vanishing contribution of the nonlinear line broadening.

To establish the relation of the observed oscillation to the characteristics of spin-wave excitations in the Py film, we determined the ferromagnetic resonance (FMR) frequency f_{FMR} by the spin torque-driven FMR (ST-FMR) technique [22]. An ac current I_{ac} was applied at a microwave frequency f_{ext} , causing magnetization oscillation due to a combination of the Oersted field and the spin torque. The resulting periodic variation of resistance due to AMR mixed with the ac current, producing a peak of dc voltage across the sample at the value of H corresponding to $f_{\text{FMR}} = f_{\text{ext}}$.

Previous studies of Pt/Py bilayers showed that the ST-FMR voltage peak contains both symmetric and antisymmetric components, due to the different contributions from the spin torque and the Oersted field of the current [11, 23]. We obtained good fits to the ST-FMR peaks with a sum of symmetric and antisymmetric Lorentzian contributions [see inset in Fig. 3(a)], allowing us to precisely determine f_{FMR} . The dependence of f_{FMR} on H agreed well with the Kittel formula, as illustrated with a solid curve in Fig. 3(a). The value $M = 827\text{ G}$ of the Py magnetization obtained from the best fit was consistent with the published data for Py [11, 23].

The maximum of the auto-oscillation frequency [triangles in Fig. 3(a)] was always lower than f_{FMR} [circles in Fig. 3(a)]. At $T = 6\text{ K}$ and $H = 350\text{ Oe}$, the auto-

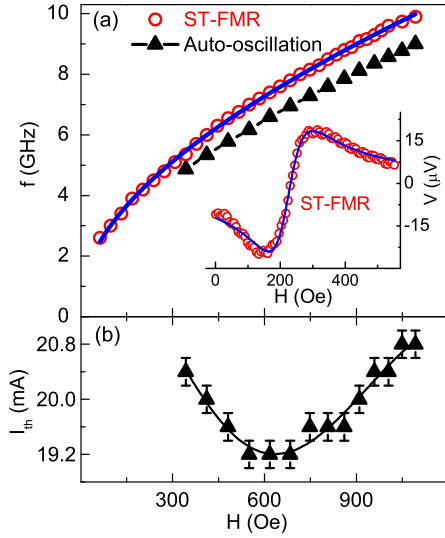


FIG. 3: (Color online). Relation of the oscillation to the ferromagnetic resonance (FMR) of the Py film. All the data were obtained at $T = 6$ K. (a) The ST-FMR frequency (circles) and the maximum auto-oscillation frequency (triangles) vs H . The solid curve is the result of fitting of the FMR data with the Kittel formula $f = \gamma \sqrt{H(H + 4\pi M)}$, where $M = 827$ G is the best-fit value for the Py magnetization, and $\gamma = 2.8$ MHz/Oe is the gyromagnetic ratio. Inset: the ST-FMR voltage vs field H obtained with ac current of 2.5 mA at frequency $f_{ext} = 4.5$ GHz. The curve is the best fit with a sum of a symmetric and an antisymmetric Lorentzian functions. (b) Dependence of the oscillation onset current I_{th} on the magnetic field. The solid curve is a guide for the eye.

oscillation frequency was 0.5 GHz lower than f_{FMR} . The difference between the two frequencies increased with increasing H , and reached 0.9 GHz at $H = 1.1$ kOe. This relationship between the oscillation and FMR was preserved at higher temperatures. Therefore, we can conclude that the auto-oscillation mode does not belong to the spin-wave spectrum, but instead forms a non-propagating self-localized "bullet" below the spin-wave spectrum [24], consistent with the results of BLS measurements in a similar device geometry [15].

The observed dependence of the oscillation threshold current I_{th} on the magnetic field [Fig. 3(b)] can be attributed to the effects of radiation damping. At $H > 600$ Oe, the value of I_{th} decreases with decreasing field, as expected for the dependence of spin torque effect on the oscillation frequency [3]. However, at $H < 600$ Oe, I_{th} starts increasing with decreasing H . The increase at small H likely originates from the decreasing frequency gap between the bullet mode and the spectrum of propagating spin-waves. Because of the thermal line broadening, there is a finite probability for the relaxation of the self-localized oscillation into the propagating spin-wave modes at close frequencies [25, 26]. Therefore, the smaller is the frequency gap, the stronger is the thermal emission

from the bullet mode, and consequently the higher is I_{th} .

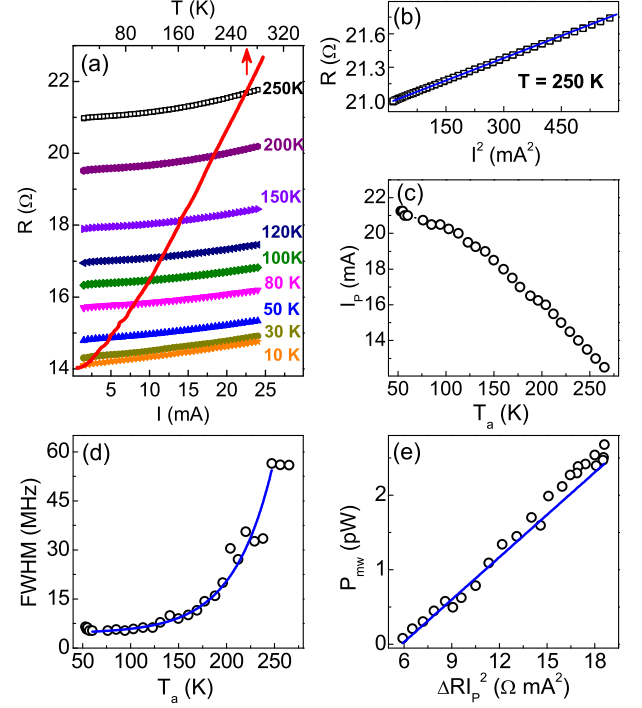


FIG. 4: (Color online). Effects of temperature on the auto-oscillation. (a) R vs I at different substrate temperatures, as labeled, (bottom axis) and R vs T measured with a small ac current (top axis). (b) R vs I^2 at 250 K. Solid line is a linear fit to the data. (c) The dependence of the current value at the maximum oscillation frequency on the calculated temperature T_a of the active device area. (d) Dependence of the linewidth at the maximum oscillation frequency on T_a . Solid curve is the result of fitting using an exponential dependence $a + b \cdot \exp(T_a/c)$ with parameters $a = 4.5$ MHz, $b = 0.13$ MHz and $c = 41.3$ K. (e) Total emitted microwave power at the maximum oscillation frequency vs $\Delta R I_p^2$. Solid line is a fit to the data.

Measurements of oscillations at different temperatures indicate significant effects of thermal fluctuations on all the oscillation characteristics, as illustrated in Fig. 4. To take into account the contribution of the Joule heating effects to the actual temperature T_a of the active device area, we first measured the dependence of the device resistance on current at different values of T , as illustrated by a series of curves in Fig. 4(a). The R vs I curves were approximately linear at cryogenic temperatures and parabolic at high temperature [see R vs I^2 plot in Fig. 4(b) for $T = 250$ K], as expected for the Joule heating effects of the active device area [27]. By comparing these dependencies to the R vs T dependence acquired with a small ac current that produces negligible heating [red curve and top scale in Fig. 4(a)], we can obtain the dependence of T_a on I at a given T . For instance, this procedure yields $T_a = 50$ K at $T = 6$ K, $I = 20$ mA for the oscillation spectrum shown in Fig. 1(b).

We now analyze the dependence of the oscillation characteristics on the temperature T_a of the active device area. The precise value of the oscillation threshold current and the oscillation characteristics at this current are difficult to determine at high temperatures due to the thermal noise. Therefore, we focus our analysis on the behaviors at the maximum of the oscillation frequency [e.g. $I = 19$ mA at $T = 120$ K in Fig. 2]. Not only is it a well-defined point of the current-dependent oscillation, but it is also characterized by the smallest generation linewidth since the nonlinear line broadening effects are minimized [21].

Figure 4(c) shows the temperature dependence of the current I_P corresponding to the maximum oscillation frequency. The value of I_P decreases from 21.2 mA at $T_a = 50$ K to 12.5 mA at $T_a = 265$ K. We observed a similar temperature dependence for the threshold current. Excitation efficiency can increase at higher temperatures due to a decrease of Py magnetization, an increase of the SHE efficiency, and/or a decrease of the dynamical damping. Our measurements of ST-FMR did not show a significant variation of f_{FMR} with temperature, indicating that the magnetization of Py does not significantly vary over the studied temperature range. We also expect that the damping of oscillation increases with increasing T , due to the larger contribution of thermal radiation of the propagating spin-wave modes. Therefore, the observed behaviors can be attributed to an increase of the SHE efficiency. A significant dependence of SHE on temperature may indeed be expected due to the temperature-dependent proximity magnetism in Pt [28, 29].

Figure 4(d) shows the dependence of the linewidth on T_a at $I = I_P$. The linewidth remains approximately constant at small T_a , and rapidly increases at $T_a > 200$ K. This dependence can be empirically fitted with an exponential function [solid curve in Fig. 4(d)]. The observed exponential increase of the linewidth with temperature is in a stark contrast with linear or \sqrt{T} dependence predicted by the theory of thermal broadening [21, 30] and observed in other magnetic auto-oscillators [22].

In contrast to the traditional spin-valve oscillators, oscillations disappeared above $T_a = 265$ K, indicating that the increased thermal radiation damping completely suppresses the auto-oscillation. Oscillation induced by SHE was observed by BLS at RT in a similar device with a larger electrode separation of 100 nm [15]. It is likely that thermal radiation effects decrease with increasing excitation area, extending the temperature range of oscillation to RT. Future analyses and experimental studies of the dependence of oscillation characteristics on the device geometry will likely clarify the origin of these behaviors.

Despite a significant nonlinear variation of the excitation current and the linewidth, the integrated emitted power P_{mw} followed a simple linear dependence on $\Delta R I_P^2$, where both I_P and ΔR vary due to their temperature dependence [Fig. 4(e)]. Nevertheless, this de-

pendence deviates from the one expected for a constant oscillation amplitude, since the value of $P_{mw}/\Delta R I_P^2$ does not remain constant due to the offset of the linear dependence in Fig. 4(e).

To summarize, we have demonstrated emission of coherent microwaves due to magnetization oscillation induced by a local pure spin current in a Py/Pt bilayer. The spin current is generated by the spin Hall effect in Pt, and the observed microwave emission is caused by the anisotropic magnetoresistance of Py. The oscillation frequency was always lower than the frequency of the ferromagnetic resonance, confirming that the oscillation mode is a self-localized standing wave. The dependence of the oscillation characteristics on current was remarkably similar to the spin-valve nano-oscillators. However, their variation with temperature was different from the traditional magnetic nano-oscillators, indicating a significant temperature dependence of both the spin Hall effect and of the magnetization dynamics. Oscillators driven by pure spin currents provide significant potential benefits compared to the traditional spin valve-based spin torque nano-oscillators, since they can utilize non-conducting magnetic layers, and their efficiency is not limited by the magnitude of the angular momentum of electron.

This work was supported by the NSF Grant ECCS-1218419.

-
- [1] G. A. Prinz, Science **282**, 1660 (1998).
 - [2] J. A. Katine, F. J. Albert, R. A. Buhrman, E. B. Myers, and D. C. Ralph, Phys. Rev. Lett. **84**, 3149 (2000).
 - [3] J. C. Slonczewski, J. Magn. Magn. Mater., **159**, L1-L7 (1996); J. Magn. Magn. Mater., **195**, L261-L268 (1999).
 - [4] L. Berger, Phys. Rev. B, **54**, 9353(1996); J. Appl. Phys., **90**, 4632 (2001).
 - [5] M. Tsoi, A. G. M. Jansen, J. Bass, W.-C. Chiang, V. Tsoi, P. Wyder, Nature, **406**, 46 (2000).
 - [6] S.I. Kiselev, J.C. Sankey, I.N. Krivorotov, N.C. Emley, R.J. Schoelkopf, R.A. Buhrman, D.C. Ralph, Nature, **425**, 380 (2003).
 - [7] T. Silva and M. Keller, IEEE Trans. Magn., **46**, 3555 (2010).
 - [8] M. I. Dyakonov and V. I. Perel, Sov. Phys. JETP Lett **13**, 467 (1971).
 - [9] J. E. Hirsch, Phys. Rev. Lett. **83**, 1834 (1999).
 - [10] K. Ando, S. Takahashi, K. Harii, K. Sasage, J. Ieda, S. Maekawa, and E. Saitoh, Phys. Rev. Lett. **101**, 036601 (2008).
 - [11] L. Liu, T. Moriyama, D. C. Ralph, and R. A. Buhrman, Phys. Rev. Lett. **106**, 036601 (2011).
 - [12] V. E. Demidov, S. Urazhdin, E. R. J. Edwards, M. D. Stiles, R. D. McMichael, and S. O. Demokritov, Phys. Rev. Lett **107**, 107204 (2011).
 - [13] Z. H. Wang, Y. Y. Sun, M. Z. Wu, V. Tiberkevich, and A. Slavin, Phys. Rev. Lett. **107**, 146602 (2011).
 - [14] L. Liu, O. J. Lee, T. J. Gudmundsen, D. C. Ralph, and R. A. Buhrman, Phys. Rev. Lett. **109**, 096602 (2012).
 - [15] V. E. Demidov, S. Urazhdin, H. Ulrichs, V. Tiberkevich,

- A. Slavin, D. Baither, G. Schmitz, and S. O. Demokritov, *Nature Mat.* in press (2012).
- [16] R.C. O’Handley, *Modern magnetic materials: principles and applications*, (Wiley-Interscience, 1999).
 - [17] Q. Mistral, Joo-Von Kim, T. Devolder, P. Crozat, and C. Chappert, J. A. Katine and M. J. Carey, and K. Ito, *Appl. Phys. Lett.* **88**, 192507 (2006).
 - [18] P. Tabor, V. Tiberkevich, A. Slavin, and S. Urazhdin, *Phys. Rev. B* **82**, 020407 (2010).
 - [19] S. Urazhdin, V. Tiberkevich, and A. Slavin, *Phys. Rev. Lett.* **105**, 237204 (2010).
 - [20] Joo-Von Kim, Q. Mistral, C. Chappert, V. Tiberkevich, and A. N. Slavin, *Phys. Rev. Lett.* **100**, 167201 (2008).
 - [21] A. Slavin and V. Tiberkevich, *IEEE Trans. Magn.* **44**, 1916 (2008); *ibid* **45**, 1875 (2009).
 - [22] G.D. Fuchs, J.C. Sankey, V.S. Pribyl, L. Qian, P.M. Braganca, A.G.F. Garcia, E.M. Ryan, Z.-P. Li, O. Ozatay, D.C. Ralph, and R.A. Buhrman, *Appl. Phys. Lett.* **91**, 062507 (2007).
 - [23] O. Mosendz, J. E. Pearson, F.Y. Fradin, G. E.W. Bauer, S. D. Bader, and A. Hoffmann, *Phys. Rev. Lett.* **104**, 046601 (2010).
 - [24] A. Slavin and V. Tiberkevich, *Phys. Rev. Lett.* **95**, 237201 (2005).
 - [25] A. N. Slavin and V. S. Tiberkevich, *Phys. Rev. B* **74**, 104401 (2006).
 - [26] S. M. Rezende, F. M. de Aguiar, R. L. Rodriguez-Surez, and A. Azevedo, *Phys. Rev. Lett.* **98**, 087202 (2007).
 - [27] R. Holm, *Electric Contacts* (Springer-Verlag, Berlin, 1967), p. 63.
 - [28] W.L. Lim, N. Ebrahim-Zadeh, H.G.E. Hentschel, S. Urazhdin, arXiv:1209.1802 (2012).
 - [29] S.Y. Huang, X. Fan, D. Qu, Y. P. Chen, W. G. Wang, J. Wu, T.Y. Chen, J. Q. Xiao, and C. L. Chien. *Phys. Rev. Lett.* **109**, 107204 (2012)
 - [30] Joo-Von Kim, V. Tiberkevich, and A. N. Slavin, *Phys. Rev. Lett.* **100**, 017207 (2008).